# Detecting Gravitational Wave Memory in the Next Galactic Core-Collapse Supernova

Colter J. Richardson,[1,*] Haakon Andresen,[2] Anthony Mezzacappa,[1] Michele Zanolin,[3] Michael G. Benjamin,[1] Pedro Marronetti,[4] Eric J. Lentz,[1,5] and Marek J. Szczepańczyk[6]

[1] *Department of Physics and Astronomy, University of Tennessee, Knoxville, TN 37996, USA*
[2] *The Oskar Klein Centre, Department of Astronomy, AlbaNova, SE-106 91 Stockholm, Sweden*
[3] *Embry-Riddle Aeronautical University, 3700 Willow Creek Road, Prescott, Arizona 86301, USA*
[4] *Physics Division, National Science Foundation, Alexandria, Virginia 22314, USA*
[5] *Physics Division, Oak Ridge National Laboratory, P.O. Box 2008, Oak Ridge, Tennessee 37831-6354, USA*
[6] *Faculty of Physics, University of Warsaw, Ludwika Pasteura 5, 02-093 Warszawa, Poland*

(Dated: April 3, 2024)

We present an approach to detecting (linear) gravitational wave memory in a Galactic core-collapse supernova *using current interferometers*. Gravitational wave memory is an important prediction of general relativity that has yet to be confirmed. Our approach uses a combination of Linear Prediction Filtering and Matched-Filtering. We present the results of our approach on data from core-collapse supernova simulations that span a range of progenitor mass and metallicity. We are able to detect gravitational wave memory out to 10 kpc. We also present the False Alarm Probabilities assuming an On-Source Window compatible with the presence of a neutrino detection.



*Introduction* The deaths of massive stars in core-collapse supernovae (CCSNe) are promising sources of gravitational waves (GWs). Stellar core collapse, core bounce at super-nuclear densities, fluid instabilities in the newly-formed proto-neutron star and in the cavity between the proto-neutron star surface and the supernova shock wave, believed to be vital to the explosive central engine, as well as explosion itself and anisotropic neutrino emission, are all expected to generate GWs [1–3]. The fluid instabilities, as well as the turbulence they induce, are expected to excite GW emission at frequencies between 50 Hz and a few kHz [4–64].

Detection strategies for CCSN GWs until now relied on excess-energy methods because the stochastic nature of the signals impeded the use of matched filtering. However, it has been pointed out recently that matched filtering alongside multi-messenger observations can improve the detection efficiency of nearby events [55]. Besides emissions above 50 Hz, a slowly evolving signal component, associated with the GW (linear) memory, is expected below a few 10's of Hz [6, 10, 11, 13, 15, 16, 18, 21, 28, 36, 41, 58–60, 65–73]. The memory in a CCSN stems from asymmetric emission of neutrinos during the explosion and the non-spherical expansion of the supernova blast wave. Although this low-frequency component contributes minimally to the total energy emitted, its amplitude can be several times larger than that of the emission above 50 Hz. Strictly speaking, the memory only refers to a constant offset in the strain after the GW pulse has passed. However, in our discussion of the memory we include the secular ramp-up to the saturation value. In terms of detectability, the GW memory from CCSNe has been largely overlooked due to the limited sensitivity of current GW detectors below 10 Hz. Moreover, even if the peak of the frequency band of the memory (including the secular ramp-up) is below 10 Hz, there may be a detectable strain (or energy) present at and above 10 Hz.

In this Letter, we demonstrate that the slow and regular time evolution of the memory is uniquely suited to matched-filter techniques. We show how matched-filtering can be utilized to detect the GW memory from CCSNe *in current interferometers*. Observing the memory, or signs of it, would confirm an important prediction of general relativity that has yet to be confirmed.

*Models* We study the memory from three state-of-the-art, three-dimensional core-collapse supernova simulations. The simulations were carried out with the Chimera [74] code, initiated from three non-rotating progenitors with zero-age main sequence masses of 9.6, 15, and 25 Solar masses, and zero and Solar metallicity [58]. The models are labeled by a "D" (for Chimera D-series simulations) followed by the mass of the progenitor from which the simulation in the series was initiated. Rapid shock expansion sets in at ∼125 ms, ∼250 ms, and ∼500 ms for D9.6, D25, and D15, respectively.

*Gravitational Wave Signals* The solid lines in the top panel of Fig. 1 show the plus polarization mode of the combined (matter and neutrino) GW strains ($h_+$) from our three models: the blue, orange, and green curves represent D25, D15, and D9.6, respectively. Within a spherical coordinate system centered on the simulations, the models are observed at randomly-chosen directions: D9.6 at $\phi = -35°$, $\theta = 90°$; D15 at $\phi = 60°$, $\theta = 70°$; and D25 at $\phi = 35°$, $\theta = 0°$. The GW signals of all three models show the slow ramp-up to a non-zero strain value that is characteristic of the memory. (Note, the D9.6 model is representative of low-mass CCSNe, which typically have low ejecta asymmetry.)

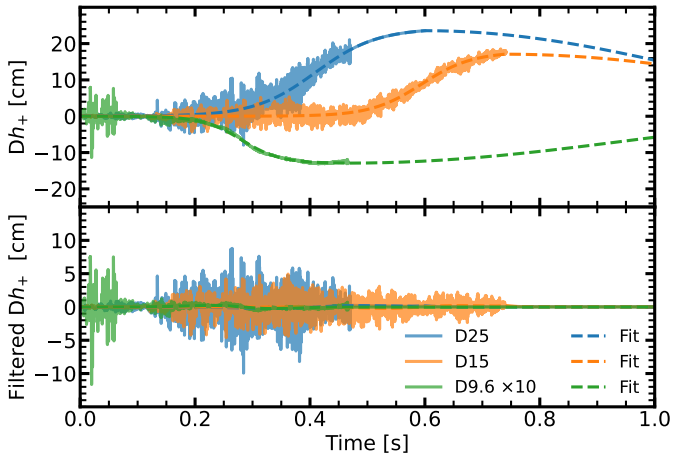


FIG. 1. Gravitational wave signals from all three models. Solid lines show the signals from the simulations. Dashed lines show the fit of the waveforms to a logistic function with a tapering (see Eq. 1 and Table I). Tapering reduces the high-frequency noise induced by the abrupt end of the simulations. We taper with a frequency of 1/10 Hz. The top panel displays unfiltered signals; the bottom panel shows the same signals with an 8 Hz high-pass Butterworth filter applied. The D9.6 signal is scaled up by a factor of 10.

*Analytical Fit* To isolate the memory, we fit the signal to a tapered logistic function defined as follows:

$$h^{\rm fit}(t) = \frac{L}{1+e^{-k(t-t_0)}}(1-H(t-t_s)) + \frac{L}{2}\big(1+\cos\left(2\pi f_t(t-t_s)\right)\big)H(t-t_s). \quad (1)$$

Here $t_0$ is the center of the rise time, $k$ is the inverse of the typical rise time, $L$ is the memory saturation value, $t_s$ is the time of saturation (or the end time of the simulation), and $H(t)$ is the Heaviside step function. The tapering is characterized by the tapering frequency, $f_t$, which we chose based on the noise characteristics of the LIGO-Virgo-Kagra (LVK) detectors. Current ground-based detectors have a sharp increase in their characteristic noise at approximately 10 Hz. As long as the tapering is longer than 0.1 s, the small amount of energy added by the tapering is negligible compared to the noise. In reality the signals are expected to saturate at some non-zero value, but we taper the signals to avoid inducing high-frequency noise in our Fourier analysis. The dashed curves in the top panel of Fig. 1 show the fits. See Table 1 for the fit parameters. For the D9.6 and D15 models, we start the tapering right as the simulations end. On the other hand, we extrapolate the D25 signal until it saturates (details regarding extrapolating the signals can be found in [72]). We extrapolate the signal from D25 because applying the tapering directly after the end of the simulation led to a discontinuity in the signal's derivative. The extrapolation is conservative and is not instrumental to detecting the actual signal.

TABLE I. The parameters used for the fit and tapering of the GW signals from the simulations (see Eq.1). Each row corresponds to a particular model.

| Model | $t_0$ $[s]$ | $L$ $[cm]$ | $k$ $[Hz]$ | $t_s$ $[s]$ | $f_t$ $[Hz]$ |
|---|---|---|---|---|---|
| D9.6 | 0.28 | -1.30 | 29.45 | 0.300 | 0.1 |
| D15 | 0.60 | 17.73 | 22.60 | 0.7414 | 0.1 |
| D25 | 0.41 | 24.23 | 18.73 | 0.472 | 0.1 |

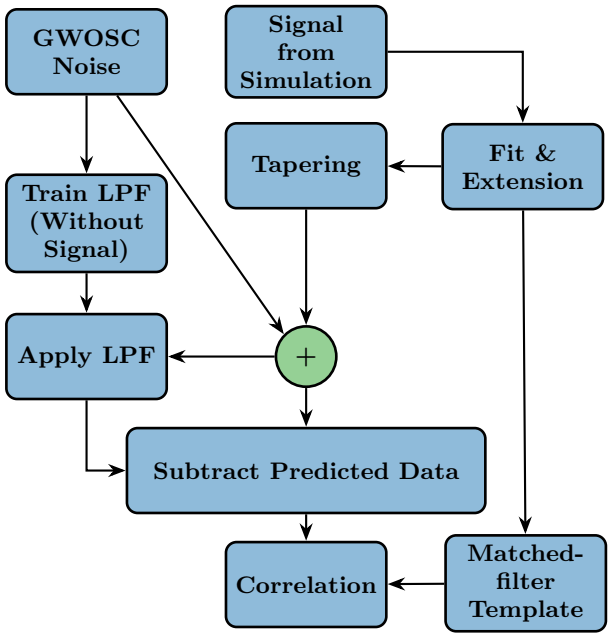


FIG. 2. Flow chart outlining the procedure presented in this Letter. The end node labeled "Correlation" corresponds to the final result of our analysis and is what we show in Fig. 4.

*Matched Filtering* The procedure implemented in this Letter, starting from the GWOSC noise data and the waveforms predicted by our simulations, is outlined in Fig.2.

We inject the tapered signals into a sample of LVK data obtained from the Gravitational Wave Open Science Center (GWOSC) [75]—specifically, a 4096 s segment of data from the O3b run of the Livingston and Hanford detectors, with an initial GPS time of 1262178304. Due to the nature of the publicly available data from GWOSC, which has a high-pass filter already applied to it, after injection we apply to the strain a high-pass Butterworth filter with a cut-off of 8 Hz. The second panel of Fig. 1 shows the signals and the fits after the filter has been applied. For all of the models, the secular ramp-up is reduced, but not erased.

After injecting the signal, we train a Linear Prediction Filter (LPF) [76, 77] with 16384 trained parameters on a 2048 s segment of the data that does not contain the signal. We then subtract the portion of the signal predicted

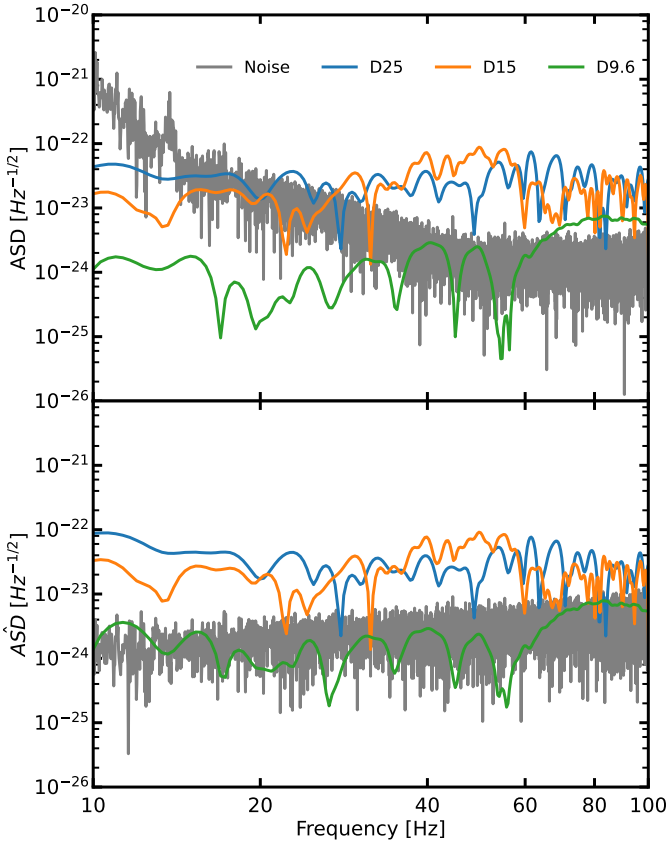


FIG. 3. Top: The Amplitude Spectral Density of: 1) the noise data from the Livingston detector (gray) and 2) of the three signals (colored lines). Bottom: The Amplitude Spectral Density of: 1) the detector noise with the part predicted by the LPF subtracted (gray) and 2) the whitened signals. Signals were scaled to a source distance of 1kpc. (colored lines)

by the LPF and define

$$\hat{S} = S - S_{\rm LPF}, \tag{2}$$

where $S$ is the strain from the detector, including the injected signal, and $S_{\rm LPF}$ is the output of the LPF. In Fig. 3 we show the amplitude spectral density (ASD) of the noise and the signals. The top (bottom) panel shows the data before (after) applying the LPF. The data in the bottom panel are defined in Eq. 2, and, for the purpose of the plots only, we assume a source distance of 1 kpc. The filtered data do not represent the actual detector strain, but by predicting, and then removing the predicted portion of the noise, we are able to better locate the memory component. The LPF below 200 Hz improves detectability metrics (like the SNR or cross-correlations with templates) for the memory by several orders of magnitude. It does affect the signal as well, but to a far lesser degree. Therefore, $\hat{S}$ is a better starting point for our matched filtering than the actual strain data.

We then calculate the discrete correlation—i.e., the *match*—between $\hat{S}$ and $h^{\rm fit}$, which is defined as follows:

$$\langle \hat{S}, h^{\rm fit} \rangle (t_n) = \sum_m \hat{S}(t_m) h^{\rm fit}(t_{m-n}). \tag{3}$$

Here we sum over all $t_m$ in our data, and $t_n$ refers to the $n$-th sample time. We simulate a two-detector network by evaluating

$$\langle \hat{S}, h^{\rm fit} \rangle^{\rm N} = \langle \hat{S}, h^{\rm fit} \rangle^{\rm H} \cdot \langle \hat{S}, h^{\rm fit} \rangle^{\rm L}, \tag{4}$$

where $\langle \hat{S}, h^{\rm fit} \rangle^{\rm H}$ and $\langle \hat{S}, h^{\rm fit} \rangle^{\rm L}$ represent $\langle \hat{S}, h^{\rm fit} \rangle$ calculated with data from the LIGO Hanford and LIGO Livingston detectors, respectively. A detector network reduces the number of false alarms by enabling coincident analysis.

For a Galactic CCSN, timing information based on a detected neutrino event would enable us to significantly narrow our search window. Assuming that the on-source window can be reduced to two seconds, we split the 4096 s window into two-second segments and define the FAP as the ratio between the number of segments with triggers above some threshold versus the total number. We leave a more complete exploration of the impact of detector networks to future work.

When performing matched filtering, the sharp edges of noise segments at the beginning and the end of a data stream can lead to large and nonphysical correlations (edge effects). Therefore, we apply a window to the noise data before our matched search. We used a Tukey window of the same length as our noise, with a shape parameter $\alpha = 0.2$.

Lastly, we note that the signals are injected at a randomly-chosen time and that choosing a different injection time does not change the general conclusions of this work. However, for the noise data we use, there are three clusters where the amplitude of the correlation, which is at its base an inner product, is large, at roughly 750 s, 894 s, and 1350 s. Injecting the signals near the noise clusters slightly decreases the efficiency of our approach. For a source distance of 10 kpc, the False Alarm Probability (FAP) increases by a few percent, but signals can still be clearly identified.

*Results* The matched-filter results for all three models, with a source distance of 10 kpc and using a two-detector network at O3b sensitivity (for the expected design sensitivity of O5, we expect at least a 50% increase), are presented in Fig. 4. The top, middle, and bottom panels correspond to models D9.6, D15, and D25, respectively. The signals were injected at one randomly-chosen time, indicated by gray dashed lines. The signals from D15 and D25 are identifiable, but the weak signal of D9.6 is not visible in the detector noise. In addition to the signal, our matched-filter approach picks out several other noise events (for example around 750 and 2656 s, see Fig.4). However, the correlations between the filtered template and noise events are smaller than

the correlation between the template and the actual signal (except for D9.6). To calculate a FAP we select a match threshold and only consider events with a correlation, $\langle \hat{S}, h^{\rm fit}\rangle^{\rm N}(t_n)/\langle \hat{S}, h^{\rm fit}\rangle^{\rm N}(t_{inj})$, higher than the chosen threshold as potential detection candidates. The threshold is chosen to achieve a desired FAP (for brevity we leave for future studies the discussion of varying the template parameters while performing the matched filtering, even if our tests indicate that this will have a small impact on the FAP curves).

For the D15 signal injected at 10 kpc, the correlation has two distinct peaks, one at the injection site and one at a glitch. This glitch is not present in either the D9.6 or the D25 case, indicating that this noise event only correlates with the D15 template. Using a threshold of 0.8, we see that the signal is one of two triggers, resulting in a FAP of 50%. While we apply a mask that removes the categorized glitches (provided by the GWOSC), a more in-depth analysis of the noise may remove these features. Lowering the threshold to 0.5 results in six triggers, leading to a FAP of 83.33%. For the D25 signal, applying the same 0.8 and 0.5 thresholds, we detect no false triggers at the higher threshold and one false trigger at the lower threshold, achieving FAPs of $\leq 1/2048$ (0.05%) and 50%, respectively.

Given a coincident neutrino detection (or a search with a two-second temporal window), Fig. 5 shows how the FAP depends on the chosen match threshold and the distance to the source. The blue, orange, and green curves correspond to models D25, D15, and D9.6, respectively. Different markers indicate different distances: 1 kpc (dots), 10 kpc (triangles), and 100 kpc (squares). At a distance of 1 kpc, the memory in the D15 and D25 models is detectable with a FAP less than 0.05% for any match threshold, while for the D9.6 model, a large match threshold is required in order to obtain similar results. (N.B. Our results at $O(1)$ kpc reflect the results we can expect at $O(10)$ kpc given next-generation detectors.) At 10 kpc, both D15 and D25 have a FAP of less than 5% for a match threshold of 0.3. For D9.6, the FAP curve does not change relative to the 1 kpc case. This occurs when, at the injection distance, the signal becomes dominated by the noise, rendering the quantity plotted in Fig. 4 independent of the distance. This would eventually happen for the D15 and D25 models, as well, at some distance above 100 kpc. At 100 kpc, a FAP for models D15 and D25 below 5-10% is possible, but only at match thresholds approaching 1.0. At a threshold of 1.0, the FAP for both models is greater than 0.05%, which means at this distance there are always triggers stronger than the injected signal. Note, the FAP curves for the D9.6 model and at large distances for models D15 and D25 (e.g., at 100 kpc) will vary with injection times, and will require potentially larger match thresholds at those distances.

*Conclusions* In this Letter, we have shown that, given the secular ramp-up of the linear GW memory in a CCSN and given the use of a Linear Prediction Filter, a matched-template search (similar to the current detection strategy for binary mergers) can be performed to detect the memory *using current interferometers* and for the first time confirm an important prediction of general relativity.

With a focus on detecting CCSNe, we have shown that, in the absence of a multimessenger detection, our approach would be effective out to a distance of 10 kpc. Of course, at these distances a multimessenger detection is expected. The detection range afforded by our approach is perhaps best discussed in the context of next-

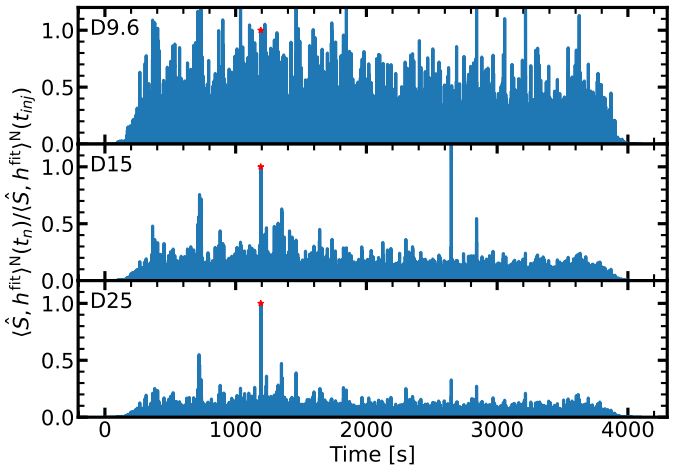


FIG. 4. The two-detector correlation (Eq. 4) between the filtered templates (bottom panel of Fig 1) and the whitened detector data. The top, middle, and bottom panels correspond to signals from the D9.6, D15, and D25 models, respectively, all at a distance of 10 kpc. The vertical gray dashed lines indicate the location of injection.

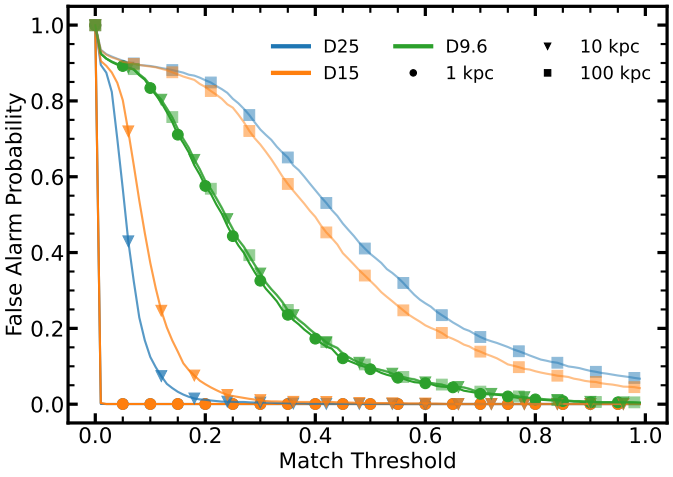


FIG. 5. The False Alarm Probability as a function of the correlation threshold used to classify a trigger. Different line markers indicate different source distances, and the colors correspond to different models.

generation interferometers. For the Einstein Telescope and Cosmic Explorer, the combination of their reduced noise floor across all frequencies, which is projected to be approximately one order of magnitude in magnitude across the sensitivity band, and the reduction of the low-frequency wall from 10 Hz to below 10 Hz, may enable the detection range of CCSNe—specifically, through the detection of GW memory—out to *Mpc distance scales*, necessarily without a concurrent neutrino detection.

While this does not impact our main conclusions, in future publications we will discuss the variability of the results using different saturation levels for the memory (as a detection and parameter estimation template search). Recent findings suggest that we can have saturation values up to 60 times larger than our signals [60], and even larger for GRBs [78], potentially extending the detection range to several Mpc *in current detectors*. Additionally, it has been found that asymmetric neutrino emission can lead to large neutron star kicks, with potential amplification through neutrino flavor conversion [79, 80]. Such large, neutrino-induced kicks would imply a substantial GW memory, detectable at far greater distances than our current signals suggest.

*Acknowledgements* H.A. is supported by the Swedish Research Council (Project No. 2020-00452). A.M. acknowledges support from the National Science Foundation's Gravitational Physics Theory Program through grants PHY-1806692 and PHY 2110177. M.Z. is supported by the National Science Foundation Gravitational Physics Experimental and Data Analysis Program through award PHY-2110555. P.M. is supported by the National Science Foundation through its employee IR/D program.

This research has made use of data or software obtained from the Gravitational Wave Open Science Center (gwosc.org), a service of the LIGO Scientific Collaboration, the Virgo Collaboration, and KAGRA. This material is based upon work supported by NSF's LIGO Laboratory, which is a major facility fully funded by the National Science Foundation, as well as the Science and Technology Facilities Council (STFC) of the United Kingdom, the Max-Planck-Society (MPS), and the State of Niedersachsen/Germany for support of the construction of Advanced LIGO and construction and operation of the GEO600 detector. Additional support for Advanced LIGO was provided by the Australian Research Council. Virgo is funded, through the European Gravitational Observatory (EGO), by the French Centre National de Recherche Scientifique (CNRS), the Italian Istituto Nazionale di Fisica Nucleare (INFN) and the Dutch Nikhef, with contributions by institutions from Belgium, Germany, Greece, Hungary, Ireland, Japan, Monaco, Poland, Portugal, and Spain. KAGRA is supported by the Ministry of Education, Culture, Sports, Science, and Technology (MEXT), the Japan Society for the Promotion of Science (JSPS) in Japan, the National Research Foundation (NRF) and Ministry of Science and ICT (MSIT) in Korea, and the Academia Sinica (AS) and National Science and Technology Council (NSTC) in Taiwan.

* cricha80@vols.utk.edu

[1] K. Kotake and T. Kuroda, Gravitational Waves from Core-Collapse Supernovae, in *Handbook of Supernovae*, edited by A. W. Alsabti and P. Murdin (2017) p. 1671.
[2] E. Abdikamalov, G. Pagliaroli, and D. Radice, Gravitational Waves from Core-Collapse Supernovae, in *Handbook of Gravitational Wave Astronomy* (2022) p. 21.
[3] A. Mezzacappa and M. Zanolin, Gravitational Waves from Neutrino-Driven Core Collapse Supernovae: Predictions, Detection, and Parameter Estimation, arXiv e-prints , arXiv:2401.11635 (2024), arXiv:2401.11635 [astro-ph.HE].
[4] E. Mueller, Gravitational radiation from collapsing rotating stellar cores, A&A **114**, 53 (1982).
[5] R. Moenchmeyer, G. Schaefer, E. Mueller, and R. E. Kates, Gravitational waves from the collapse of rotating stellar cores., A&A **246**, 417 (1991).
[6] E. Mueller and H. T. Janka, Gravitational radiation from convective instabilities in Type II supernova explosions., A&A **317**, 140 (1997).
[7] H. Dimmelmeier, J. A. Font, and E. Müller, Gravitational Waves from Relativistic Rotational Core Collapse, ApJ **560**, L163 (2001), arXiv:astro-ph/0103088 [astro-ph].
[8] K. Kotake, S. Yamada, and K. Sato, Gravitational radiation from axisymmetric rotational core collapse, Phys. Rev. D **68**, 044023 (2003), arXiv:astro-ph/0306430 [astro-ph].
[9] K. Kotake, S. Yamada, K. Sato, K. Sumiyoshi, H. Ono, and H. Suzuki, Gravitational radiation from rotational core collapse: Effects of magnetic fields and realistic equations of state, Phys. Rev. D **69**, 124004 (2004), arXiv:astro-ph/0401563 [astro-ph].
[10] E. Müller, M. Rampp, R. Buras, H. T. Janka, and D. H. Shoemaker, Toward Gravitational Wave Signals from Realistic Core-Collapse Supernova Models, ApJ **603**, 221 (2004), arXiv:astro-ph/0309833 [astro-ph].
[11] K. Kotake, W. Iwakami, N. Ohnishi, and S. Yamada, Stochastic Nature of Gravitational Waves from Supernova Explosions with Standing Accretion Shock Instability, ApJ **697**, L133 (2009), arXiv:0904.4300 [astro-ph.HE].
[12] A. Marek, H. T. Janka, and E. Müller, Equation-of-state dependent features in shock-oscillation modulated neutrino and gravitational-wave signals from supernovae, A&A **496**, 475 (2009), arXiv:0808.4136 [astro-ph].
[13] J. W. Murphy, C. D. Ott, and A. Burrows, A Model for Gravitational Wave Emission from Neutrino-Driven Core-Collapse Supernovae, ApJ **707**, 1173 (2009), arXiv:0907.4762 [astro-ph.SR].
[14] S. Scheidegger, R. Käppeli, S. C. Whitehouse, T. Fischer, and M. Liebendörfer, The influence of model parameters on the prediction of gravitational wave signals from stellar core collapse, Astron. Astrophys. **514**, A51 (2010).
[15] K. Kotake, W. Iwakami-Nakano, and N. Ohnishi, Effects of Rotation on Stochasticity of Gravitational Waves in

the Nonlinear Phase of Core-collapse Supernovae, ApJ **736**, 124 (2011), arXiv:1106.0544 [astro-ph.HE].

[16] E. Müller, H. T. Janka, and A. Wongwathanarat, Parametrized 3D models of neutrino-driven supernova explosions. Neutrino emission asymmetries and gravitational-wave signals, A&A **537**, A63 (2012), arXiv:1106.6301 [astro-ph.SR].

[17] P. Cerdá-Durán, N. DeBrye, M. A. Aloy, J. A. Font, and M. Obergaulinger, Gravitational Wave Signatures in Black Hole Forming Core Collapse, ApJ **779**, L18 (2013), arXiv:1310.8290 [astro-ph.SR].

[18] B. Müller, H.-T. Janka, and A. Marek, A New Multidimensional General Relativistic Neutrino Hydrodynamics Code of Core-collapse Supernovae. III. Gravitational Wave Signals from Supernova Explosion Models, ApJ **766**, 43 (2013), arXiv:1210.6984 [astro-ph.SR].

[19] C. D. Ott, E. Abdikamalov, P. Mösta, R. Haas, S. Drasco, E. P. O'Connor, C. Reisswig, C. A. Meakin, and E. Schnetter, GENERAL-RELATIVISTIC SIMULATIONS OF THREE-DIMENSIONAL CORE-COLLAPSE SUPERNOVAE, Ap.J. **768**, 115 (2013).

[20] T. Kuroda, T. Takiwaki, and K. Kotake, Gravitational wave signatures from low-mode spiral instabilities in rapidly rotating supernova cores, Phys. Rev. D **89**, 044011 (2014), arXiv:1304.4372 [astro-ph.HE].

[21] K. N. Yakunin, A. Mezzacappa, P. Marronetti, S. Yoshida, S. W. Bruenn, W. R. Hix, E. J. Lentz, O. E. Bronson Messer, J. A. Harris, E. Endeve, J. M. Blondin, and E. J. Lingerfelt, Gravitational wave signatures of ab initio two-dimensional core collapse supernova explosion models for 12 -25 $M_\odot$ stars, Phys. Rev. D **92**, 084040 (2015), arXiv:1505.05824 [astro-ph.HE].

[22] K. Hayama, T. Kuroda, K. Kotake, and T. Takiwaki, Coherent network analysis of gravitational waves from three-dimensional core-collapse supernova models, Phys. Rev. D **92**, 122001 (2015), arXiv:1501.00966 [astro-ph.HE].

[23] K. Hayama, T. Kuroda, K. Nakamura, and S. Yamada, Circular Polarizations of Gravitational Waves from Core-Collapse Supernovae: A Clear Indication of Rapid Rotation, Phys. Rev. Lett. **116**, 151102 (2016), arXiv:1606.01520 [astro-ph.HE].

[24] T. Kuroda, K. Kotake, and T. Takiwaki, A New Gravitational-wave Signature from Standing Accretion Shock Instability in Supernovae, ApJ **829**, L14 (2016), arXiv:1605.09215 [astro-ph.HE].

[25] T. Kuroda, K. Kotake, K. Hayama, and T. Takiwaki, Correlated Signatures of Gravitational-wave and Neutrino Emission in Three-dimensional General-relativistic Core-collapse Supernova Simulations, ApJ **851**, 62 (2017), arXiv:1708.05252 [astro-ph.HE].

[26] S. Richers, C. D. Ott, E. Abdikamalov, E. O'Connor, and C. Sullivan, Equation of state effects on gravitational waves from rotating core collapse, Phys. Rev. D **95**, 063019 (2017), arXiv:1701.02752 [astro-ph.HE].

[27] H. Andresen, B. Müller, E. Müller, and H.-T. Janka, Gravitational wave signals from 3d neutrino hydrodynamics simulations of core-collapse supernovae, Mon. Not. Roy. Ast. Soc. **468**, 2032–2051 (2017).

[28] V. Morozova, D. Radice, A. Burrows, and D. Vartanyan, The Gravitational Wave Signal from Core-collapse Supernovae, ApJ **861**, 10 (2018), arXiv:1801.01914 [astro-ph.HE].

[29] E. P. O'Connor and S. M. Couch, Exploring Fundamentally Three-dimensional Phenomena in High-fidelity Simulations of Core-collapse Supernovae, ApJ **865**, 81 (2018), arXiv:1807.07579 [astro-ph.HE].

[30] T. Takiwaki and K. Kotake, Anisotropic emission of neutrino and gravitational-wave signals from rapidly rotating core-collapse supernovae, MNRAS **475**, L91 (2018), arXiv:1711.01905 [astro-ph.HE].

[31] K. Hayama, T. Kuroda, K. Kotake, and T. Takiwaki, Circular polarization of gravitational waves from non-rotating supernova cores: a new probe into the pre-explosion hydrodynamics, Mon. Not. Roy. Ast. Soc. **477**, L96 (2018), arXiv:1802.03842 [astro-ph.HE].

[32] H. Kawahara, T. Kuroda, T. Takiwaki, K. Hayama, and K. Kotake, A Linear and Quadratic Time–Frequency Analysis of Gravitational Waves from Core-collapse Supernovae, Ap.J. **867**, 126 (2018), arXiv:1810.00334 [astro-ph.HE].

[33] T. Kuroda, K. Kotake, T. Takiwaki, and F.-K. Thielemann, A full general relativistic neutrino radiation-hydrodynamics simulation of a collapsing very massive star and the formation of a black hole, Mon. Not. Roy. Ast. Soc.: Letters **477**, L80 (2018).

[34] K.-C. Pan, M. Liebendörfer, S. M. Couch, and F.-K. Thielemann, Equation of state dependent dynamics and multi-messenger signals from stellar-mass black hole formation, Ap.J. **857**, 13 (2018).

[35] H. Andresen, E. Müller, H. T. Janka, A. Summa, K. Gill, and M. Zanolin, Gravitational waves from 3D core-collapse supernova models: The impact of moderate progenitor rotation, MNRAS **486**, 2238 (2019), arXiv:1810.07638 [astro-ph.HE].

[36] D. Radice, V. Morozova, A. Burrows, D. Vartanyan, and H. Nagakura, Characterizing the Gravitational Wave Signal from Core-collapse Supernovae, ApJ **876**, L9 (2019), arXiv:1812.07703 [astro-ph.HE].

[37] D. Vartanyan, A. Burrows, D. Radice, M. A. Skinner, and J. Dolence, A successful 3D core-collapse supernova explosion model, Mon. Not. Roy. Ast. Soc. **482**, 351 (2019), arXiv:1809.05106 [astro-ph.HE].

[38] V. Srivastava, S. Ballmer, D. A. Brown, C. Afle, A. Burrows, D. Radice, and D. Vartanyan, Detection prospects of core-collapse supernovae with supernova-optimized third-generation gravitational-wave detectors, Phys. Rev. D **100**, 043026 (2019), arXiv:1906.00084 [gr-qc].

[39] J. Powell and B. Müller, Gravitational wave emission from 3d explosion models of core-collapse supernovae with low and normal explosion energies, Mon. Not. Roy. Ast. Soc. **487**, 1178 (2019).

[40] A. Mezzacappa, P. Marronetti, R. E. Landfield, E. J. Lentz, K. N. Yakunin, S. W. Bruenn, W. R. Hix, O. E. B. Messer, E. Endeve, J. M. Blondin, and J. A. Harris, Gravitational-wave signal of a core-collapse supernova explosion of a 15 $M_\odot$ star, Phys. Rev. D **102**, 023027 (2020), arXiv:2007.15099 [astro-ph.HE].

[41] J. Powell and B. Müller, Three-dimensional core-collapse supernova simulations of massive and rotating progenitors, MNRAS **494**, 4665 (2020), arXiv:2002.10115 [astro-ph.HE].

[42] S. Shibagaki, T. Kuroda, K. Kotake, and T. Takiwaki, A new gravitational-wave signature of low-T/—W— instability in rapidly rotating stellar core collapse, MNRAS **493**, L138 (2020), arXiv:1909.09730 [astro-ph.HE].

[43] M. L. Warren, S. M. Couch, E. P. O'Connor, and V. Mo-

rozova, Constraining properties of the next nearby core-collapse supernova with multimessenger signals, Ap.J. **898**, 139 (2020).

[44] D. Vartanyan and A. Burrows, Gravitational Waves from Neutrino Emission Asymmetries in Core-collapse Supernovae, Astrophys. J. **901**, 108 (2020), arXiv:2007.07261 [astro-ph.HE].

[45] H. Andresen, R. Glas, and H. T. Janka, Gravitational-wave signals from 3D supernova simulations with different neutrino-transport methods, MNRAS **503**, 3552 (2021), arXiv:2011.10499 [astro-ph.HE].

[46] O. Andersen Eggenberger, S. Zha, A. da Silva Schneider, A. Betranhandy, S. M. Couch, and E. P. O'Connor, Equation-of-state Dependence of Gravitational Waves in Core-collapse Supernovae, ApJ **923**, 201 (2021), arXiv:2106.09734 [astro-ph.HE].

[47] M. A. Pajkos, M. L. Warren, S. M. Couch, E. P. O'Connor, and K.-C. Pan, Determining the Structure of Rotating Massive Stellar Cores with Gravitational Waves, ApJ **914**, 80 (2021), arXiv:2011.09000 [astro-ph.HE].

[48] S. Shibagaki, T. Kuroda, K. Kotake, and T. Takiwaki, Characteristic time variability of gravitational-wave and neutrino signals from three-dimensional simulations of non-rotating and rapidly rotating stellar core collapse, Mon. Not. Roy. Ast. Soc. **502**, 3066 (2021), arXiv:2010.03882 [astro-ph.HE].

[49] K.-C. Pan, M. Liebendörfer, S. M. Couch, and F.-K. Thielemann, Stellar mass black hole formation and multimessenger signals from three-dimensional rotating core-collapse supernova simulations, Ap.J. **914**, 140 (2021).

[50] T. Kuroda, T. Fischer, T. Takiwaki, and K. Kotake, Core-collapse Supernova Simulations and the Formation of Neutron Stars, Hybrid Stars, and Black Holes, ApJ **924**, 38 (2022), arXiv:2109.01508 [astro-ph.HE].

[51] J. Matsumoto, Y. Asahina, T. Takiwaki, K. Kotake, and H. R. Takahashi, Magnetic support for neutrino-driven explosion of 3D non-rotating core-collapse supernova models, Mon. Not. Roy. Ast. Soc. **516**, 1752 (2022), arXiv:2202.07967 [astro-ph.HE].

[52] K. Nakamura, T. Takiwaki, and K. Kotake, Three-dimensional simulation of a core-collapse supernova for a binary star progenitor of SN 1987a, Mon. Not. Roy. Ast. Soc. **514**, 3941 (2022).

[53] J. Powell and B. Müller, Inferring astrophysical parameters of core-collapse supernovae from their gravitational-wave emission, Phys. Rev. D **105**, 063018 (2022), arXiv:2201.01397 [astro-ph.HE].

[54] M. Bugli, J. Guilet, T. Foglizzo, and M. Obergaulinger, Three-dimensional core-collapse supernovae with complex magnetic structures - II. Rotational instabilities and multimessenger signatures, MNRAS **520**, 5622 (2023), arXiv:2210.05012 [astro-ph.HE].

[55] M. Drago, H. Andresen, I. Di Palma, I. Tamborra, and A. Torres-Forné, Multimessenger observations of core-collapse supernovae: Exploiting the standing accretion shock instability, Phys. Rev. D **108**, 103036 (2023), arXiv:2305.07688 [astro-ph.HE].

[56] P. Jakobus, B. Müller, A. Heger, S. Zha, J. Powell, A. Motornenko, J. Steinheimer, and H. Stöcker, Gravitational Waves from a Core g Mode in Supernovae as Probes of the High-Density Equation of State, Phys. Rev. Lett. **131**, 191201 (2023), arXiv:2301.06515 [astro-ph.HE].

[57] T. Kuroda and M. Shibata, Spontaneous scalarization as a new core-collapse supernova mechanism and its multimessenger signals, Phys. Rev. D **107**, 103025 (2023), arXiv:2302.09853 [astro-ph.HE].

[58] A. Mezzacappa, P. Marronetti, R. E. Landfield, E. J. Lentz, R. D. Murphy, W. Raphael Hix, J. A. Harris, S. W. Bruenn, J. M. Blondin, O. E. Bronson Messer, J. Casanova, and L. L. Kronzer, Core collapse supernova gravitational wave emission for progenitors of 9.6, 15, and 25 $M_\odot$, Phys. Rev. D **107**, 043008 (2023), arXiv:2208.10643 [astro-ph.SR].

[59] M. A. Pajkos, S. J. VanCamp, K.-C. Pan, D. Vartanyan, N. Deppe, and S. M. Couch, Characterizing the Directionality of Gravitational Wave Emission from Matter Motions within Core-collapse Supernovae, ApJ **959**, 21 (2023), arXiv:2306.01919 [astro-ph.HE].

[60] D. Vartanyan, A. Burrows, T. Wang, M. S. B. Coleman, and C. J. White, Gravitational-wave signature of core-collapse supernovae, Phys. Rev. D **107**, 103015 (2023), arXiv:2302.07092 [astro-ph.HE].

[61] C. Afle, S. K. Kundu, J. Cammerino, E. R. Coughlin, D. A. Brown, D. Vartanyan, and A. Burrows, Measuring the properties of f -mode oscillations of a protoneutron star by third-generation gravitational-wave detectors, Phys. Rev. D **107**, 123005 (2023), arXiv:2304.04283 [astro-ph.IM].

[62] T. Bruel, M.-A. Bizouard, M. Obergaulinger, P. Maturana-Russel, A. Torres-Forné, P. Cerdá-Durán, N. Christensen, J. A. Font, and R. Meyer, Inference of protoneutron star properties in core-collapse supernovae from a gravitational-wave detector network, Phys. Rev. D **107**, 083029 (2023), arXiv:2301.10019 [astro-ph.HE].

[63] Z. Lin, A. Rijal, C. Lunardini, M. D. Morales, and M. Zanolin, Characterizing a supernova's standing accretion shock instability with neutrinos and gravitational waves, Phys. Rev. D **107**, 083017 (2023), arXiv:2211.07878 [astro-ph.HE].

[64] C. J. Richardson, M. Zanolin, H. Andresen, M. J. Szczepańczyk, K. Gill, and A. Wongwathanarat, Modeling core-collapse supernovae gravitational-wave memory in laser interferometric data, Phys. Rev. D **105**, 103008 (2022), arXiv:2109.01582 [astro-ph.HE].

[65] R. Epstein, The generation of gravitational radiation by escaping supernova neutrinos., ApJ **223**, 1037 (1978).

[66] M. S. Turner, Gravitational radiation from supernova neutrino bursts, Nature **274**, 565 (1978).

[67] K. N. Yakunin, P. Marronetti, A. Mezzacappa, S. W. Bruenn, C. Lee, M. A. Chertkow, W. Hix, J. M. Blondin, E. J. Lentz, O. E. B. Messer, and S. Yoshida, Gravitational Waves from Core Collapse Supernovae, Class. Quant. Grav. **27**, 194005 (2010), arXiv:1005.0779.

[68] T. Takiwaki and K. Kotake, Gravitational Wave Signatures of Magnetohydrodynamically Driven Core-collapse Supernova Explosions, ApJ **743**, 30 (2011), arXiv:1004.2896 [astro-ph.HE].

[69] J. Powell and B. Müller, Gravitational wave emission from 3D explosion models of core-collapse supernovae with low and normal explosion energies, MNRAS **487**, 1178 (2019), arXiv:1812.05738 [astro-ph.HE].

[70] R. Jardine, J. Powell, and B. Müller, Gravitational wave signals from 2D core-collapse supernova models with rotation and magnetic fields, MNRAS **510**, 5535 (2022), arXiv:2105.01315 [astro-ph.HE].

[71] K. Nakamura, T. Takiwaki, and K. Kotake, Three-dimensional simulation of a core-collapse supernova for a binary star progenitor of SN 1987A, Mon. Not. Roy. Ast. Soc. **514**, 3941 (2022), arXiv:2202.06295 [astro-ph.HE].

[72] C. J. Richardson, M. Zanolin, H. Andresen, M. J. Szczepańczyk, K. Gill, and A. Wongwathanarat, Modeling core-collapse supernovae gravitational-wave memory in laser interferometric data, Phys. Rev. D **105**, 103008 (2022), arXiv:2109.01582 [astro-ph.HE].

[73] J. Powell, B. Müller, D. R. Aguilera-Dena, and N. Langer, Three dimensional magnetorotational core-collapse supernova explosions of a 39 solar mass progenitor star, MNRAS **522**, 6070 (2023), arXiv:2212.00200 [astro-ph.HE].

[74] S. W. Bruenn, J. M. Blondin, W. R. Hix, E. J. Lentz, O. E. B. Messer, A. Mezzacappa, E. Endeve, J. A. Harris, P. Marronetti, R. D. Budiardja, M. A. Chertkow, and C.-T. Lee, CHIMERA: A Massively Parallel Code for Core-collapse Supernova Simulations, ApJS **248**, 11 (2020), arXiv:1809.05608 [astro-ph.IM].

[75] R. Abbott *et al.* (KAGRA, VIRGO, LIGO Scientific), Open Data from the Third Observing Run of LIGO, Virgo, KAGRA, and GEO, Astrophys. J. Suppl. **267**, 29 (2023), arXiv:2302.03676 [gr-qc].

[76] L. B. Jackson, Discrete fourier transform, in *Digital Filters and Signal Processing: With MATLAB® Exercises* (Springer US, Boston, MA, 1996) pp. 189–248.

[77] Brian McFee, Colin Raffel, Dawen Liang, Daniel P.W. Ellis, Matt McVicar, Eric Battenberg, and Oriol Nieto, librosa: Audio and Music Signal Analysis in Python, in *Proceedings of the 14th Python in Science Conference*, edited by Kathryn Huff and James Bergstra (2015) pp. 18 – 24.

[78] G. Urrutia, F. De Colle, C. Moreno, and M. Zanolin, Gravitational waves from the propagation of long gamma-ray burst jets, MNRAS **518**, 5242 (2023), arXiv:2208.00129 [astro-ph.HE].

[79] H. Nagakura, K. Sumiyoshi, and S. Yamada, Possible Early Linear Acceleration of Proto-neutron Stars via Asymmetric Neutrino Emission in Core-collapse Supernovae, ApJ **880**, L28 (2019), arXiv:1907.04863 [astro-ph.HE].

[80] H. Nagakura and K. Sumiyoshi, Neutron star kick driven by asymmetric fast-neutrino flavor conversion, arXiv e-prints , arXiv:2401.15180 (2024), arXiv:2401.15180 [astro-ph.HE].